

Outer density profiles of 19 Galactic globular clusters from deep and wide-field imaging

Julio A. Carballo-Bello^{1,2} ^{*}, Mark Gieles³, Antonio Sollima⁴, Sergey Koposov³, David Martínez-Delgado⁵ and Jorge Peñarrubia³

¹*Instituto de Astrofísica de Canarias (IAC), Vía Láctea s/n, La Laguna E-38205, S/C de Tenerife, Spain*

²*Departamento de Astrofísica, Universidad de La Laguna, La Laguna E-38205, S/C de Tenerife, Spain*

³*Institute of Astronomy, University of Cambridge, CB3 0HA Cambridge, United Kingdom*

⁴*INAF- Observatorio Astronomico di Padova, I35122 Padova, Italy*

⁵*Max Planck Institut für Astronomie, D69117 Heidelberg, Germany*

23 April 2018

ABSTRACT

Using deep photometric data from WFC@INT and WFI@ESO2.2m we measure the outer number density profiles of 19 stellar clusters located in the inner region of the Milky Way halo (within a Galactocentric distance range of 10–30 kpc) in order to assess the impact of internal and external dynamical processes on the spatial distribution of stars. Adopting power-law fitting templates, with index $-\gamma$ in the outer region, we find that the clusters in our sample can be divided in two groups: a group of massive clusters ($\geq 10^5 M_{\odot}$) that has relatively flat profiles with $2.5 < \gamma < 4$ and a group of low-mass clusters ($\leq 10^5 M_{\odot}$), with steep profiles ($\gamma > 4$) and clear signatures of interaction with the Galactic tidal field. We refer to these two groups as ‘tidally unaffected’ and ‘tidally affected’, respectively. Our results also show a clear trend between the slope of the outer parts and the half-mass density of these systems, which suggests that the outer density profiles may retain key information on the dominant processes driving the dynamical evolution of Globular Clusters.

Key words: globular clusters: general – methods: observational – stars: Population II – techniques: photometric

1 INTRODUCTION

Globular clusters (GCs) have been found in nearly all galaxies and they have been considered the fossil records of the formation of their host galaxy (e.g. Zinn 1993; Zepf & Ashman 1993; Brodie & Strader 2006; Marín-Franch et al. 2009). In the Milky Way roughly 150 GCs are currently known (Harris 1996, 2010) and they have a long history of being used in the context of stellar evolution (e.g. Baraffe et al. 1998), the structure and chemical evolution of the Milky Way (e.g. Innanen et al. 1983; Searle & Zinn 1978, respectively) and the dynamical evolution of collisional systems (Hut et al. 1992; Meylan & Heggie 1997).

The radial number density profiles of GCs can be used to learn about their evolution because the structure and evolution of clusters are closely linked (Hénon 1961). In recent years, much attention has gone to the inner parts of the

surface brightness profile to quantify the number of clusters that has undergone core collapse (Djorgovski & King 1986) and to look for the presence of massive black holes (Noyola & Gebhardt 2006). Especially for the densest clusters, these studies require the high angular resolution of space based observatories, such as the Hubble Space Telescope, to resolve the dense core into individual stars. On the other hand, the spatial distribution of the bulk of the stars is determined by the interplay between internal and external dynamical processes. Internal relaxation processes tend to populate the outer regions of the cluster with low-mass stars, whereas the external tidal field of the host galaxy will strip some of the stars at large radii. Hence, studies of the entire profile are useful to gain insight on the overall evolution of individual clusters. Since such studies require a wide field of view, they are usually done from the ground (Trager et al. 1995, hereafter TGK95).

Several self-consistent (static) models for clusters exist, using different assumptions for the distribution function (e.g. Plummer 1911; Woolley & Robertson 1956; Michie

^{*} E-mail: jacob@iac.es

1963; King 1966; Wilson 1975). The surface brightness profile is often used to say something about the correctness of a model, but unfortunately it does not always provide enough information to constrain the underlying model, i.e. without the use of additional information such as stellar velocities. This was already noted by Hénon (1961) who realised that different models could successfully describe the surface brightness profile of a GC despite their different underlying physical assumptions.

Most of these models are based on simplifying assumptions, such as spherical symmetry, an isotropic velocity distribution, stars of the same mass and a truncation of the distribution function. It is, therefore, that empirical templates are often used, i.e. simple fitting formulas that do not (necessarily) follow from a specific distribution function, to fit and compare surface brightness profiles of clusters. A well-known example is the King (1962) template that is typically used for old GCs and that is characterised by a steep drop, or truncation, of the density at the outer edge. This radius is called the tidal radius in King's paper, but because it does not necessarily coincide with the radius of the zero-velocity surface, or Jacobi radius (Baumgardt et al. 2010; Küpper et al. 2010), we will refer to the radius where King models drop to zero density as the edge radius (r_{edge}). Elson et al. (1987, hereafter EFF87) used a continuous template (i.e. without a truncation) for relatively young clusters in the Large Magellanic Clouds (LMC). The EFF87 template is characterised by a flat core and a power-law envelope. These are part of the more general family of power-law models (Zhao 1996).

The cluster system of the LMC is a good example of how observations of the structure of clusters can be used as a proxy for evolution. Because the ages of clusters in the LMC span a range from a few Myrs to ~ 12 Gyr, variations of structural parameters with age can be studied, and when interpreting this as evolution, much can be learned. For example, Elson et al. (1989) and Mackey & Gilmore (2003b) showed that the core sizes of LMC clusters increase (on average) with age, which was also found for clusters in the Small Magellanic Clouds (SMC; Mackey & Gilmore 2003a) and for cluster systems outside the Local Group (Maíz-Apellániz 2001; Bastian et al. 2008). Numerical studies suggest that this expansion is largely driven by internal evolution (Mackey et al. 2008), rather than by external effects such as the details of the orbit around the centre of the galaxy (Wilkinson et al. 2003).

The young SMC/LMC clusters and young extra-Galactic clusters (e.g. Larsen 2004) are well described by the continuous power-law models, whereas for old GCs (tidally) truncated King models are often used. It seems, therefore, logic to conclude that clusters form with extended haloes and that a tidal truncation develops over time through interactions of the cluster with the tidal field of its host galaxy. Because the tidal field is strongest at pericentre, it is often assumed that this is where the truncation in the cluster density is determined (King 1962; Innanen et al. 1983). Numerical works, however, indicate that the reality is more complicated. Collision-less N -body simulations of stellar clusters that start with a King-type density distribution and that move on eccentric orbits in the Galactic potential develop an halo of "extra-tidal" stars as they shed a fraction of their stellar mass to tides (Johnston et al.

1999). Once the unbound material escapes and equilibrium is re-established, the outer profile of the cluster does not exhibit the original truncation and instead approaches a power-law (Oh et al. 1995; Peñarrubia et al. 2009). The surface density in that halo is shallower than for the bulk of the stars and the location where the break occurs is an indication of the time elapsed from the last pericentre passage (Peñarrubia et al. 2009). Observational examples of this phenomenon have been discovered in Pal 5 (Odenkirchen et al. 2003; Dehnen et al. 2004), NGC 5466 (Belokurov et al. 2006) and Pal 14 (Sollima et al. 2011).

Tidal stripping is not the only process that can generate a break in the surface density profile. Models of star clusters that lose stars through two-body relaxation and move on a circular orbit, i.e. without the time-dependent tides that give rise to tidal stripping, also develop a halo of energetically unbound stars. These stars were dubbed "potential escapers" and they are trapped within the Jacobi surface because the criterion for escape is not only based on energy but also on angular momentum (Fukushige & Heggie 2000; Baumgardt 2001). These stars give rise to a very similar break in the outer parts of the surface density profile as in the tidal stripping scenario (Küpper et al. 2010). Such a break was found in the surface density/brightness profiles of the GCs M 92 (Testa et al. 2000), Pal 13 (Côté et al. 2002), Whiting 1 (Carraro et al. 2007) and AM 4 (Carraro 2009). Often these breaks go together with direct detections of the characteristic "S-shaped" tidal features and/or tidal tails (Belokurov et al. 2006; Jordi & Grebel 2010; Niederste-Ostholt et al. 2010). When the details of the orbit of the cluster are not available, it is difficult, if not impossible, to disentangle the relative contributions of tidal stripping and two-body relaxation to the formation of the break in the surface brightness profile.

McLaughlin & van der Marel (2005, hereafter MvM05) fit different models to the surface brightness profiles of Milky Way GCs using the data of TGK95 and they find that the more extended Wilson (1975) and EFF87 models provide equally good and sometimes even better descriptions than the traditional King (1966) models. In particular, they show that goodness of fit parameters indicate a preference for more extended models whenever more data in the outer parts are available. They refrain from a detailed interpretation and conclude that age is not the only parameter that determines whether a King-type (i.e. truncated) model provides a good description of the surface brightness profile, or not. In this study we search for the additional ingredient driving the shape of the clusters density profiles.

This paper is organized as follows. In § 2 we present the sample of Galactic GCs included in this study and a description of the observations needed for our purposes. In § 3, we describe how we obtained the number density profiles on which this study is based and the fitting technique adopted to derive their structural parameters. In § 4 the number density profiles are presented and are interpreted in § 5 in connection with possible external and internal processes. In § 6 we draw our conclusions.

2 THE SAMPLE

The clusters included in this project are part of a study that focused on the search for tidal streams around Galactic GCs (Martínez-Delgado et al. 2004). For this purpose, we have observed a sample of 19 GCs in the Galactic halo between 10 and 30 kpc in Galactocentric distance, sampling $\sim 56\%$ of the total number of Galactic GCs in this distance range. Since photometry at low Galactic latitudes is severely hampered by the presence of field stars, we have excluded all those objects located within 20 degrees from the Galactic plane with the exception of NGC 2298 and Rup 106, which have been observed in spite of their low Galactic latitude because of their possible association with the Canis Major stream (Bellazzini et al. 2004; Forbes & Bridges 2010). Because all the GCs in our sample lie in a 20 kpc wide distance range, we can study the effect of a similar external Galactic tidal field on the structure of clusters with different properties.

To place the sample in the context of the Milky Way GC population, we show their half-mass densities, ρ_h , against the Galactocentric distance, R_G , together with the values for the rest of the GCs (Figure 1). A constant mass-to-light ratio of 2 was used for this figure and the half-mass density is defined as $\rho_h \equiv 8M/(3\pi r_h^3)$. Here M is the mass and r_h is the three-dimensional half-mass radius which is estimated from the half-light radius in projection, or effective radius (r_{eff}) by correcting for the effect of projection, i.e. $r_h = (4/3)r_{\text{eff}}$ (Spitzer 1987). This is a powerful diagram to study the relation between internal and external effects who both affect cluster properties (Innanen et al. 1983; Gieles et al. 2011). The lines are 'cluster isochrone relations' at an age of a Hubble time for clusters with different masses that evolve in a steady tidal field (Appendix B in Gieles et al. 2011). It assumes that two-body relaxation is the dominant process, which is a valid assumption for most clusters outside ~ 10 kpc (Gnedin & Ostriker 1997; Vesperini & Heggie 1997). Gieles et al. (2011) showed that clusters that form deeply embedded within their Roche-lobe spend roughly the first half of their lives in an 'expansion-dominated' phase and during the second half of their lives they are in an 'evaporation-dominated' phase. These authors considered relaxation driven evaporation of clusters on circular orbits. Because the evolution of clusters on eccentric orbits is affected by an additional tidal effect, i.e. tidal stripping, we introduce a more general reference to these two regimes, namely 'tidally unaffected' and 'tidally affected', respectively. According to Gieles et al. (2011), clusters that satisfy

$$M < 10^5 M_\odot \frac{4 \text{ kpc}}{R_G} \quad (1)$$

are in the tidally affected regime. This constraint is satisfied for $\sim 25\%$ of the clusters in our sample: Rup 106, NGC 5053, NGC 5466, Pal 5 and NGC 7492. The remaining clusters of our sample will be referred to as tidally unaffected clusters.

To derive the mass of the clusters (Table 2), we have taken the V -band mass-to-light ratios found by MvM05 and the luminosities derived from the integrated V magnitudes of our profiles¹. Moreover, trying to complete our analysis

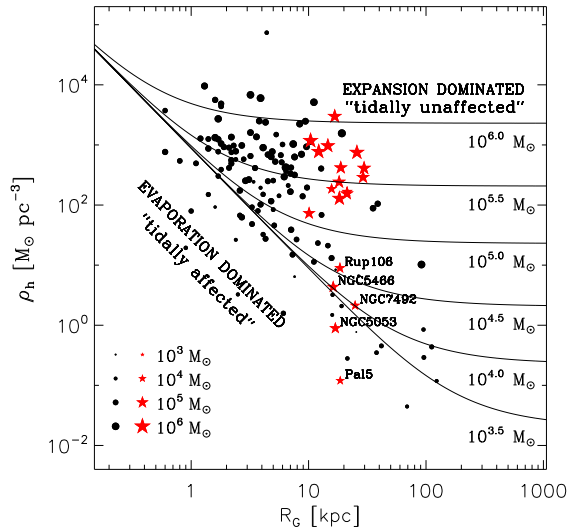


Figure 1. Half-mass densities against Galactocentric distances of the 141 globular clusters (black dots) of the Harris catalogue (Harris 1996). The clusters used in this study are highlighted with a (red) star. All symbol sizes scale with the mass of the cluster. Cluster isochrone relations from Gieles et al. (2011) are overplotted for clusters with different masses. Clusters that align with the horizontal lines are in the tidally unaffected regime, whereas clusters that align the diagonal line are in the tidally affected regime. The exact separation between these regimes is given by equation (1).

of the dynamical state of each cluster, we have used the expression

$$t_{\text{rh}} = \frac{0.138}{\bar{m} \ln(0.11M/\bar{m})} \left(\frac{Mr_h^3}{G} \right)^{1/2} \text{Myr} \quad (2)$$

by Spitzer & Hart (1971) to obtain the half-mass relaxation time in Myr. In this formula, \bar{m} is the mean stellar mass that has been set to $0.5 M_\odot$. The constant of 0.11 was found by Giersz & Heggie (1994) for clusters of equal mass stars.

The six-dimensional phase space information of a GC is essential to derive its orbit in the Galaxy and evaluate its interaction with the Milky Way tidal field. While accurate positions on the sky, distances and radial velocities are available for all the cluster of our sample, proper motions are difficult to obtain for these distant objects. We only have found orbital parameters for 10 of our GCs in the compilation by Dinescu et al. (1999). Absolute ages included in Table 1 are extracted from the database by Forbes & Bridges (2010) except for NGC 6229 (Borissova et al. 1999). Coordinates and distances are taken from the Harris catalogue (Harris 1996, 2010).

2.1 Observations

As already reported in the previous Section, the observational data used in this paper come from a photometric cam-

¹ To convert V magnitudes into luminosities we adopted the dis-

tance moduli and reddening from Harris (2010) and $M_{V,\odot} = 4.83$ (Binney & Merrifield 1998)

Cluster	$l(^{\circ})$	$b(^{\circ})$	$R_G(\text{kpc})$	$r_{\text{eff}}(^{\prime})$	Age (Gyr)	$R_{\text{apo}}(\text{kpc})$	$R_{\text{peri}}(\text{kpc})$	Telescope/Run
NGC 1261	270.54	-52.12	18.2	0.68	10.24	—	—	ESO2.2/Nov09
NGC 1851	244.51	-35.03	16.7	0.52	9.98	30.4 ± 3.9	5.7 ± 1.1	ESO2.2/Jan00
NGC 1904	227.23	-29.35	18.8	0.66	11.14	19.9 ± 1.0	4.2 ± 1.3	ESO2.2/Jan00
NGC 2298	245.63	-16.00	15.7	0.76	12.67	15.3 ± 1.0	1.9 ± 1.4	ESO2.2/Feb09
NGC 4147	252.85	77.19	21.3	0.49	11.39	25.3 ± 2.6	4.1 ± 2.2	INT/May04
Rup 106	300.88	11.67	18.5	1.05	10.20	—	—	ESO2.2/Feb09
NGC 4590	299.63	36.05	10.1	1.51	11.52	24.4 ± 3.1	8.6 ± 0.3	ESO2.2/Feb10
NGC 5024	332.96	79.76	18.3	1.32	12.67	36.0 ± 16.8	15.5 ± 1.9	INT/May04
NGC 5053	335.70	78.95	16.9	2.58	12.29	—	—	INT/May08
NGC 5272	42.22	78.71	12.2	2.37	11.39	13.4 ± 0.8	5.5 ± 0.8	INT/May10
NGC 5466	42.15	73.59	16.2	2.27	13.57	57.1 ± 24.6	6.6 ± 1.5	INT/May08
NGC 5634	342.21	49.26	21.2	0.88	11.84	—	—	ESO2.2/Feb10
NGC 5694	331.06	30.36	29.1	0.41	13.44	—	—	ESO2.2/Feb10
NGC 5824	332.56	22.07	25.8	0.46	12.80	—	—	ESO2.2/Feb10
Pal 5	0.85	45.86	18.6	2.68	9.80	15.9 ± 2.5	2.3 ± 2.3	INT/Jun01
NGC 6229	73.64	40.31	29.7	0.36	11.8	—	—	INT/Aug09
NGC 6864	20.30	-25.75	14.6	0.47	9.98	—	—	ESO2.2/May10
NGC 7078	65.01	-27.31	10.4	1.00	12.93	10.3 ± 0.7	5.4 ± 1.1	INT/Jun10
NGC 7492	53.39	-63.48	24.9	1.13	12.00	—	—	ESO2.2/Nov09

Table 1. Sample of Galactic GCs included in this project. Coordinates and distances were obtained from the updated version of Harris catalogue (Harris 1996, 2010) while radii have been inferred from the structural parameters published in MVM05, except for Rup 106, taken from Harris. Absolute ages are those computed by Forbes & Bridges (2010) except for NGC 6229 (Borissova et al. 1999) and Galactocentric distances during apo- and pericentre of the clusters are obtained from Dinescu et al. (1999).

paign aimed at searching for tidal streams around Galactic GCs. Due to the low surface brightness of known Galactic tidal streams (~ 32 mag/arcmin 2), a suitable combination of wide field and exposure time was required. We have used the Wide Field Camera (WFC) located at the Isaac Newton Telescope at the Roque de los Muchachos Observatory (La Palma, Spain) and the Wide Field Imager (WFI) at the ESO 2.2 m telescope at La Silla Observatory (Chile). The WFC covers 34×34 arcmin with 4 identical chips while the WFI has a similar field of view (FOV) of 34×33 arcmin distributed in 8 chips.

For those clusters with angular sizes comparable to the FOVs of the instruments, it was necessary to include an additional field to cover the outer regions, where we focus on. The total exposure times in B and R bands were 4×900 s and 6×600 s respectively reaching a limiting magnitude of ~ 5 mag below the turn-off in the colour-magnitude diagram (CMD). With such deep photometry we have been able to detect cluster members in the outer parts of these systems where the stellar density is critically low.

The images were processed using the *imred* package and standard routines in IRAF. Photometry was obtained with the PSF-fitting algorithm of DAOPHOT II/ALLSTAR (Stetson 1987). One of the main advantages of using this software is that it provides criteria to reject extended objects as background galaxies so we only included stellar-shaped objects in our final photometric catalogue. This decision is taken based on the sharpness parameter for which we set the limitation $|\text{sh}| \leq 0.5$. During each observing run a set of photometric standard stars from the catalogue by Landolt (1992) have been observed. They have been used to derive the transformation between the instrumental magnitude and the standard Johnson system. We adopted the atmospheric extinction coefficients provided by both observatories.

3 NUMBER DENSITY PROFILES. FITTING

To construct the radial density profiles, we selected the bona-fide cluster members along the main-sequence (MS). First, we fitted the CMD of each cluster with a set of isochrones from Marigo et al. (2008) with suitable age and metallicity from Forbes & Bridges (2010) and adopting the distance and reddening by Harris (2010). We defined a box in the CMD containing all the stars with $|(B-R)_{\text{iso}} - (B-R)_{\text{cmd}}| \leq 0.15$ and $B_{\text{to}} \leq B \leq B_{\text{max}}$, where $(B-R)_{\text{iso}}$ and $(B-R)_{\text{cmd}}$ are the isochrone and stars colours, respectively, B_{to} the turn-off magnitude and B_{max} a limiting magnitude defined to be $2.23 \leq B_{\text{max}} - B_{\text{to}} \leq 4.48$ depending on the cluster. The adopted magnitude range represents a good compromise to maximize the number of cluster objects ensuring a good level of completeness ($\phi \geq 90\%$) estimated from artificial star experiments in the most crowded region used in the analysis for a subsample of relatively dense GCs (see Bellazzini et al. 2002). The comparison with the theoretical isochrones indicates that in all the GCs of our sample, the stars that satisfy the adopted selection criterion lie in a similar mass range, between $0.77 \leq M_{\text{max}} \leq 0.86 M_{\odot}$ and $0.52 \leq M_{\text{min}} \leq 0.69 M_{\odot}$, where M_{max} and M_{min} are the maximum and minimum stellar masses found in the MS of these clusters. Although the adopted selection criteria in both sharpness and location in the CMD minimize the contamination from back/foreground field stars and galaxies, the presence of some intruders in the sample is unavoidable. The fraction of contaminating objects has been estimated for a subsample of clusters for which suitable control fields located at the same Galactic latitude but ~ 3 deg away from the cluster position. We estimated a fraction of outliers satisfying the selection criteria described above of 0.1-0.3%. Moreover, such objects are expected to be homogeneously

distributed across the field of view and should therefore not alter significantly the profile shape. So, we can can safely consider negligible the effect of such intruders in the derived profiles.

We counted all those stars included in our box that are contained in concentric annuli, centred in the cluster centre coordinates with fixed width in logarithmic scale. The number of counts per unit area has been obtained by dividing the number of stars that satisfy the above criteria by the corresponding area covered by the annuli. The area of each annulus has been corrected for the region not covered by our observations (gaps between the chips, borders truncation, ect). The error on the density has been estimated using the standard error propagation formula and assuming a Poisson statistic for star counts.

For most of the clusters of our sample the half-mass relaxation time is smaller than their age. It is therefore important to investigate the effect that mass segregation could have on the resulting profiles by splitting the MS in two subsamples of equal magnitude extent covering different magnitude ranges. We found no signs of significant differences in the obtained density profiles for all the clusters of our sample along the entire cluster extent, with $\Delta n(r) \leq 1.5\%$ (see Figure 2 for the illustrative case of NGC 1904). The Kolmogorov-Smirnov test indicates a probability of $\sim 98\%$ that the radial profiles obtained for the two different subsamples of MS stars are extracted from the same population. So we can neglect the effects that mass segregation could have on our derived profiles.

The long exposure times needed to reach a lower limiting magnitude while allowing to efficiently study the outer region of these GCs, causes severe incompleteness in the inner arcminutes which prevent us from studying the structure in the innermost portion of the cluster. As a solution, we have used the catalogue of surface brightness profiles of GCs in the Milky Way published by TGK95 (with the exception of Rup 106, not included in that catalogue). For each cluster we have converted the TGK95 profiles into star counts adopting the relation

$$n(r) = C - 0.4 \mu_V(r) \quad (3)$$

Then we fitted both our and the TGK95 dataset simultaneously, leaving the vertical scaling factor between the two profiles, C , as a free parameter in the fitting model.

In the fitting procedure we optimized the combined chi-square (χ^2) of both datasets. When fitting, we noticed that certain profiles in the TGK95 dataset have a fraction of points with very small (probably unrealistic) error-bars, which would completely drive the fit. Furthermore, in several cases, the data from TGK95 in the very inner parts of the clusters show some small scale structure in the profiles, which can be either intrinsic or due to systematic effects. In order for the fit to be determined mainly by the overall profile shape rather than a few points/structures in the TGK95 data, we decided to limit the smallest error-bar of the TGK95 dataset to 0.1 dex in density.

The fitting model for the profiles was:

$$n(r) = n_{\text{BG}} + n_{\text{cl}}(r) \quad (4)$$

where n_{BG} is the density of background/foreground sources and $n_{\text{cl}}(r)$ is the model for the cluster density profile. In this paper we considered two different models. As in

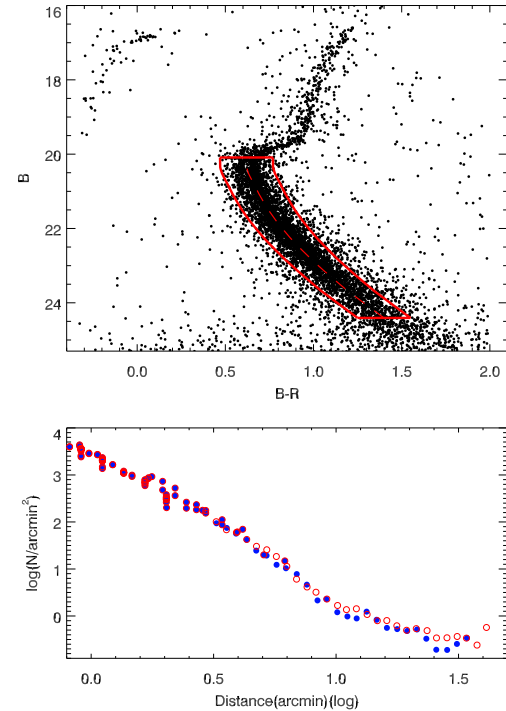


Figure 2. Example of MS stars selection to calculate the number density profile of the cluster NGC 1904. The lower panel shows the profiles for different masses ranges ($0.68 \leq M \leq 0.83 M_{\odot}$, open red circles; $0.54 \leq M \leq 0.68 M_{\odot}$, solid blue circles).

EFF87, a power-law model with parameter γ controlling the shape of the profile :

$$n_{\text{cl}}(r) = n_0 \frac{1}{(1 + (r/r_0)^2)^{\gamma/2}} \quad (5)$$

and the King (1996) profile, parametrized by the W_0 parameter:

$$n_{\text{cl}}(r) = n_0 \times F(r, r_0, W_0) \quad (6)$$

Because King (1966) models do not have an analytical solution for the surface density, a grid of models was pre-computed by numerical solving the Poisson equation.

In order to fit the density profiles, instead of standard gradient descent methods (e.g. Levenberg-Marquardt), we decided to employ a Markov Chain Monte-Carlo (MCMC) technique to better explore the possible covariance between parameters. For each cluster, we ran multiple MCMC chains, and then from all the chains we picked up the values of the parameters giving a best fit to the data, while the 1D posterior distributions of the parameters gave us estimates of the error-bars, which were often large due to the covariance between them. Since our data combined with the TGK95 data covers very large range of radii, for a few clusters we do see systematic deviations of the observed profiles from our simple models. In these cases obviously the error-bars on the parameters are only indicative. In a few cases the background is not well sampled by our density profiles. In our fitting procedure, the sky level is a free parameter with a flat prior between 0 and the average of a few outer points of the density profile. This parameter is sampled by the MCMC

chain and the values of all the free parameters have been determined from marginalized 1D posteriors, so the errors on the structural parameters are in some cases significantly influenced by the errors of the sky determination.

4 RESULTS

The derived number density profiles are shown in Figures 3 to 7. In order to obtain a better vision of the divergences between the King (blue dashed line) and power-law (red solid line) fittings, we have included the profiles both in logarithmic and linear scales in the left and right panel, respectively. We have also indicated the start point of our data with an arrow pointing down, whereas upward pointing arrow indicates the last data point of the TGK95 profile for each cluster (with the exception of Rup 106 which is not contained in that study).

The tidal radii previously estimated by MvM05 for these clusters are marked in the profiles as vertical dashed lines. For most of the cases, the known tidal radius does not seem to be compatible with the profiles obtained in this work. In clear cases as NGC 1851, NGC 5824 or NGC 6229, the distance at which the truncation on the profile is expected using the TGK95 profiles alone seems to be located within the continuous power-law profile found in our data set. This fact shows the risk of computing these parameters from FOV-limited photometry.

Since in our power-law model $n_{\text{cl}}(r) \propto r^{-\gamma}$ for large distances from the cluster centre, the parameter γ represents the slope of the outer regions of the profiles and we can use it as an indicator of the overall shape of the profile. To have a better vision of the variation of the number density profiles in connection with the physical properties contained in Table 2, they have been sorted in ascending order of γ .

It is visible both in the density profiles and the information shown in Table 2, that the tidally affected clusters NGC 7492, NGC 5466, Pal 5, NGC 5053 and Rup 106 are the low-density subsample with steeper profiles. The effects that variable tides have in the overall structure of these clusters is evident with the appearance of breaks in the outer parts profiles in some of the clusters, with NGC 5466 and Pal 5 as best examples. We also know of the existence of more or less coherent tidal tails emerging from NGC 5053 (Lauchner et al. 2006), NGC 5466 (Belokurov et al. 2006), Pal 5 (Odenkirchen et al. 2001) and NGC 7492 (Leon et al. 2000). In this context, the shallower profile observed in the outer regions of NGC 5466, Pal 5 and possibly NGC 7492 is generated by the dramatic impact that tidal stripping has in populating the outskirts of the cluster. Given that the second slope beyond the break only modifies slightly the global profile, we proceed with the analysis of these clusters in the same conditions as the rest of the sample.

On the other hand, massive clusters and more generally denser systems, present a relatively flatter profile with a remarkable continuous power-law distribution. This group coincides with what we here refer to as tidally unaffected clusters and in these cases we do not detect any signal of tidal truncation on the profiles or the existence of potential tidal debris as in the low-density group.

Using the γ parameter as an indicator of the overall structure, we conclude that, as a general rule, tidally affected

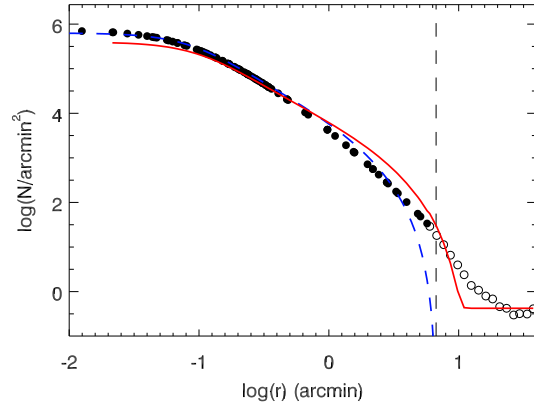


Figure 8. King model fit for NGC 1851. The fit made using only TGK95 data (black dots) and the combined sample constructed adding the densities measured in this work (open dots) are shown with red solid and blue dashed lines respectively. Vertical line indicates the position of the edge radius derived by MvM05.

clusters present $\gamma > 4$ while the tidally unaffected group is confined to the range $2.5 < \gamma < 4$. This agrees with the profile obtained for an isolated M31 GC by Mackey et al. (2010), which ranges from $\gamma = -2.5$ in the inner parts to $\gamma = -3.5$ far from the cluster centre. It is also interesting to note the coincidence with the result presented by Baumgardt et al. (2010), where the existence of two populations in the Galactic GCs was found, based on the ratio of their half-mass to Jacobi radii. Our tidally affected (tidally unaffected) clusters are referred to as tidally filling (compact) in that work.

We want to remark the problems that King model has to describe the profiles of NGC 1851, NGC 5272, NGC 5824 and NGC 7078, four of the most massive clusters included in our sample, as well as NGC 5466, NGC 5694 or NGC 6229. In the case of NGC 7078 it is not surprising since (as NGC 1904) is classified as core-collapsed GC in the Djorgovski & King (1986) catalogue. In all the other cases, the inclusion of our data in the outermost part of the clusters drives the fit towards small core radii and the failure of the King model in describing the overall cluster structure (see Figure 8). On the other hand, we find NGC 5634 that is clearly difficult to fit with a single power-law.

Structural parameters derived from the fitting as well the masses and half-mass densities inferred from our profiles (using a power-law description) have been included in Table 2. The uncertainties both in W_0 and γ show how important is to have the inner regions to constraint the overall results: in the extreme case, Rup 106, the lack of information of the central parts of the cluster generates problems for both models to obtain a reasonable fit.

5 DISCUSSION

5.1 Power-law template vs. King model

The number density profiles presented in this paper show that, in most of the cases, the outer parts of the clusters extend to large distances from the centre, generally beyond

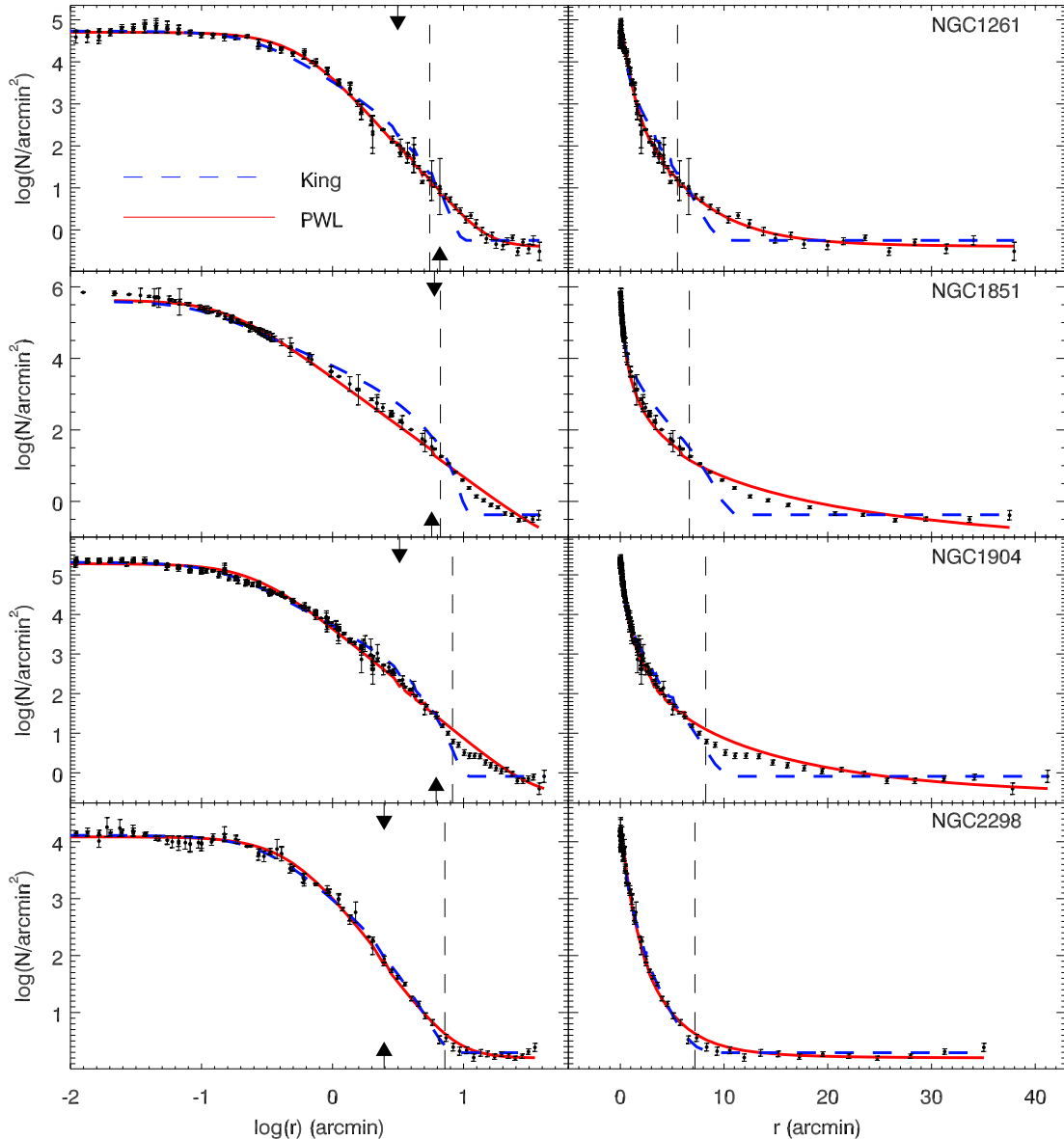


Figure 3. Number density profiles for NGC 1261, NGC 1851, NGC 1904 and NGC 2298. Blue dashed line corresponds with the best King model fitting while red line shows the best power-law fitting following the expression described in Section 3. Upper arrow shows the initial data point we have obtained from our data while lower arrow represents the last TGK95 data point. Vertical dashed line indicates the tidal radius obtained by MvM05. Note that the vertical range of the plots might differ from cluster to cluster.

the edge radius inferred from the previous studies based on datasets restricted to the innermost region. As a consequence, the systematic application of the King model to previous data and the lack of complete radial profiles seems to have generated the idea that these profiles are truncated, whereas here we show that in some cases the profile is well described by a continuous power-law down to our detection limit.

To analyse the effect that increasing the observed FOV has on the derived properties of GCs, we have plotted our

best fit γ and r_{edge} against those derived by MvM05² (which are based on the TGK95 surface brightness profiles) in Figure 9 (upper panels). From this comparison, the presence of clear trends is evident: for tidally unaffected GCs ($\gamma \leq 4$), we find slightly steeper profiles (larger γ), while for the tidally affected clusters NGC 5466, Pal 5 and NGC 7492 the profiles

² Note that MvM05 use γ to describe the power-law decline of the 3-dimensional number density profile. We, therefore, subtracted 1 from their values to be able to compare to our γ , that describes the decline of the number density profile in projection, i.e. $\gamma_{3D} = \gamma_{2D} + 1$.

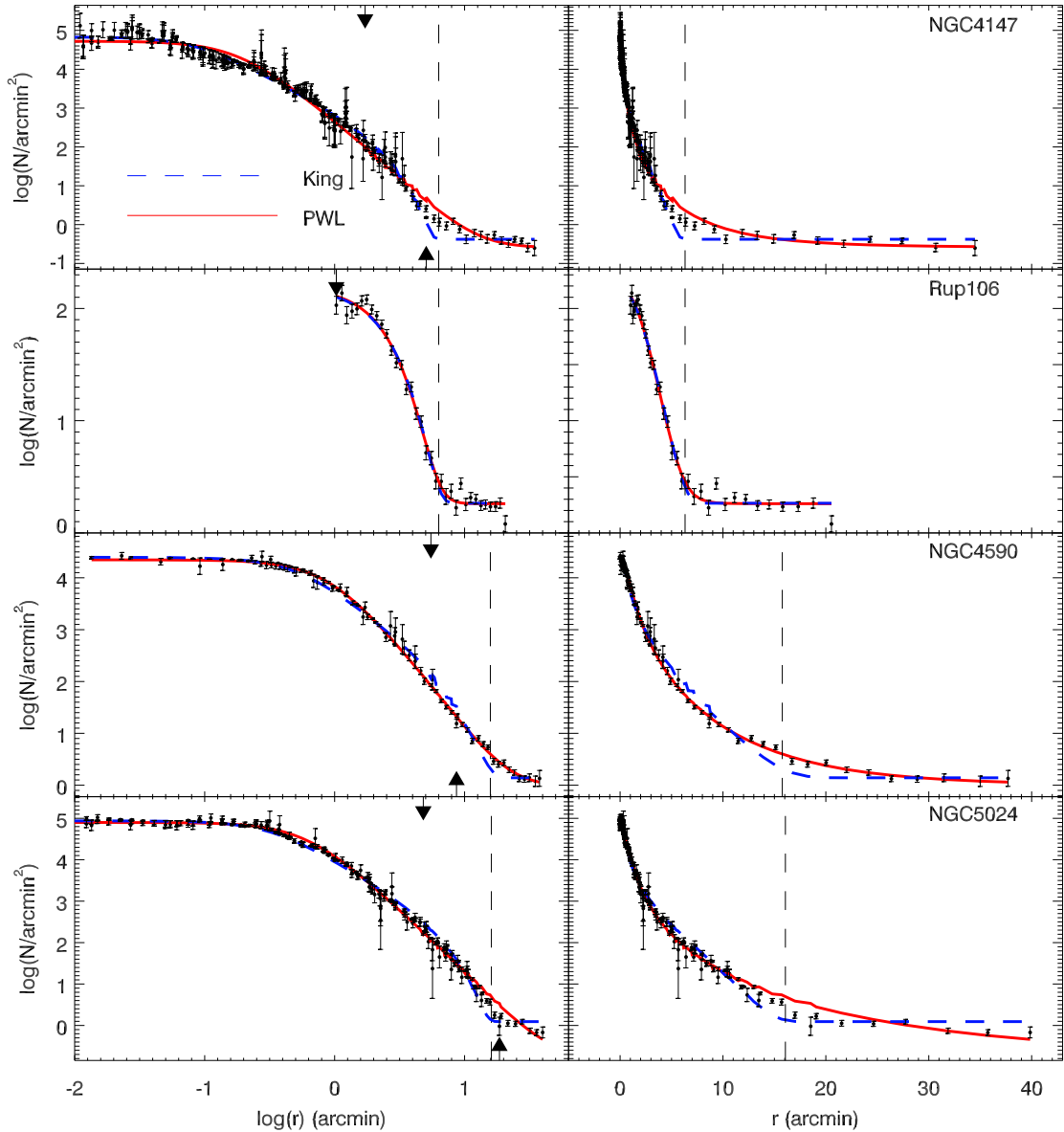


Figure 4. Same as Fig. 3 for NGC 4147, Rup 106, NGC 4590 and NGC 5024.

are slightly shallower (smaller γ). This result is expected because of the presence of tidal debris in the outermost parts of these clusters which were not contained in the original TGK95 data. New edge radii are also remarkably bigger than the previous values reported by MvM05 with a mean variation of $\sim +40\%$, excluding the 4 GCs which present smaller derived edge radii and those which are poorly fitted by King models (see below). With these new results, we do not detect signatures, at least in the tidally unaffected group, of truncation on the profiles.

To investigate the suitability of the King model and a power-law to describe our GCs, we compared the computed χ^2 . In Figure 9 we plot the rate of the χ^2 of the power-law fit, χ^2_{PL} , over the χ^2 following from the King model fit, χ^2_K , as a function of γ (bottom-left panel) and the same ratio if

we only include the TGK95 data (bottom-right panel). According to these results, the power-law template is a better approximation to the observed number density profiles for $\sim 2/3$ of the clusters in our sample with the remarkable exceptions of NGC 5634 with $\chi^2_{\text{PL}}/\chi^2_K \geq 3$. Again, the density profiles of the tidally affected clusters (with the exception of NGC 5053) are better reproduced by power-law fits. The same result can be found also using only the inner part of the profile from TGK95. It is interesting to note the striking difference in the $\chi^2_{\text{PL}}/\chi^2_K$ ratio of NGC 6864 (member of the tidally unaffected group of clusters) which is better fitted by a King model when only the inner region is considered, while showing a power-law shape when the entire profile is considered.

The reason for the deviation from the King model pro-

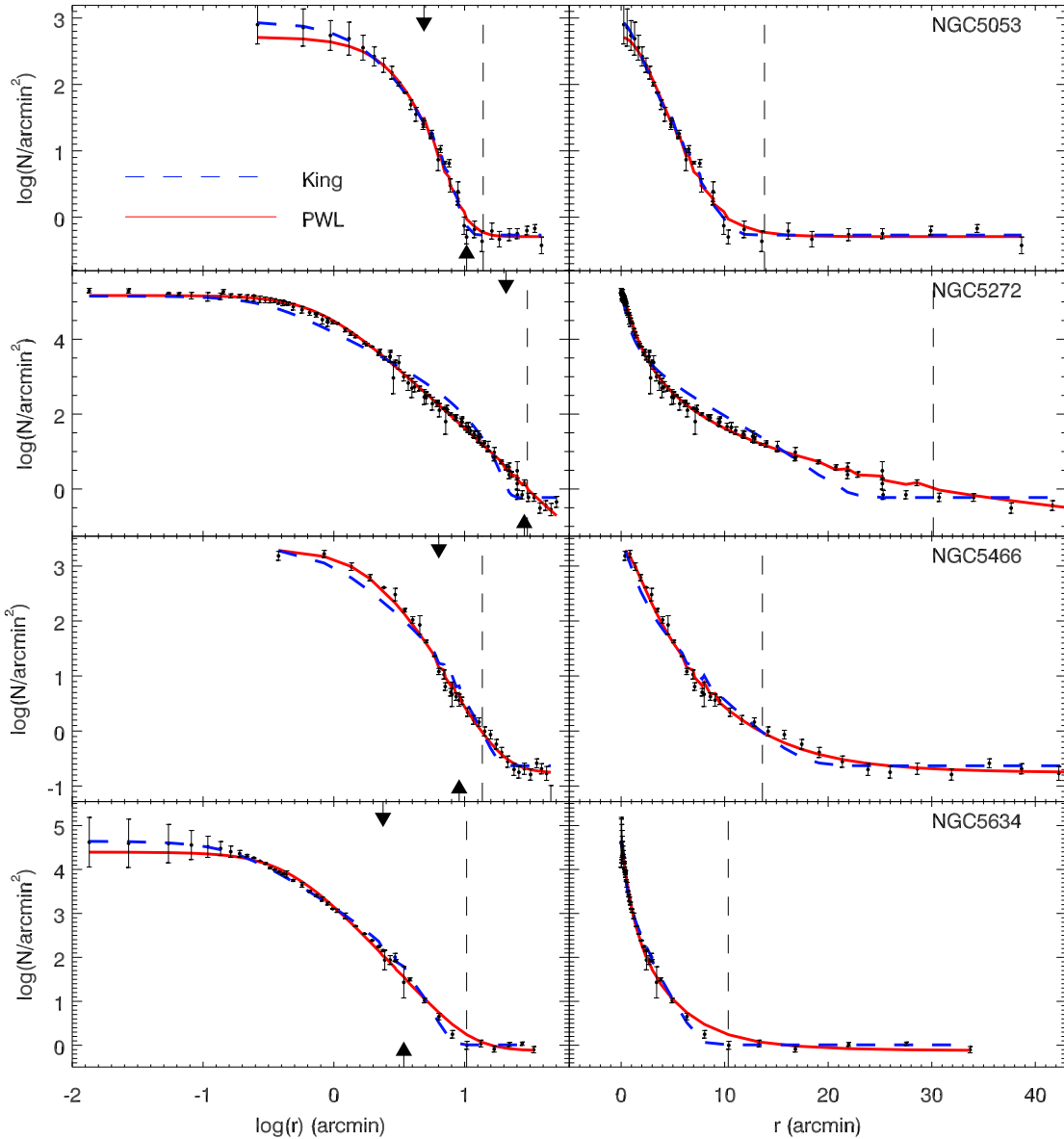


Figure 5. Same as Fig. 3 for NGC 5053, NGC 5272, NGC 5466 and NGC 5634.

file in the group of tidally affected GCs can be found in the working hypothesis made in King (1966) models on the radial truncation at the zero-energy surface. In fact, while stars with energy above the critical energy (i.e. a velocity larger than the local escape velocity) are actually expected to evaporate from the cluster, in real clusters they remain marginally bound to the system for a timescale comparable to the cluster orbital period around the parent galaxy (Lee & Ostriker 1987), or even longer (Fukushige & Heggie 2000). This effect produces a significant overdensity of stars in the outermost regions of the cluster with respect to the prediction of a King model without affecting the inner profile (see also Johnston et al. 1999). This effect is more evident in clusters in the evaporation regime (i.e. tidally affected) and those subject to a stronger interaction with the exter-

nal tidal field. The assumption of the King edge radius as a real physical limit of the cluster, leads to the use of the term 'extra-tidal stars' for those cluster members outside this radius. This has been confirmed in several GCs during the last years, with NGC 1851 (Olszewski et al. 2009), IC 4499 (Walker et al. 2011) or NGC 5694 (Correnti et al. 2011) as recent examples, and can be noticed also in an important part of our profiles (see Figures 3 to 7). Of course, despite of the above limitations, King models remain a valid representation of a GC (at least in the inner part of the profile). However, because the power-law template is a reasonable choice to describe the derived number density profiles, we decided to use the outer slope γ as an indicator of the overall structure of our target GCs in the following sections. The main consequence of assuming a power-law as the best tem-

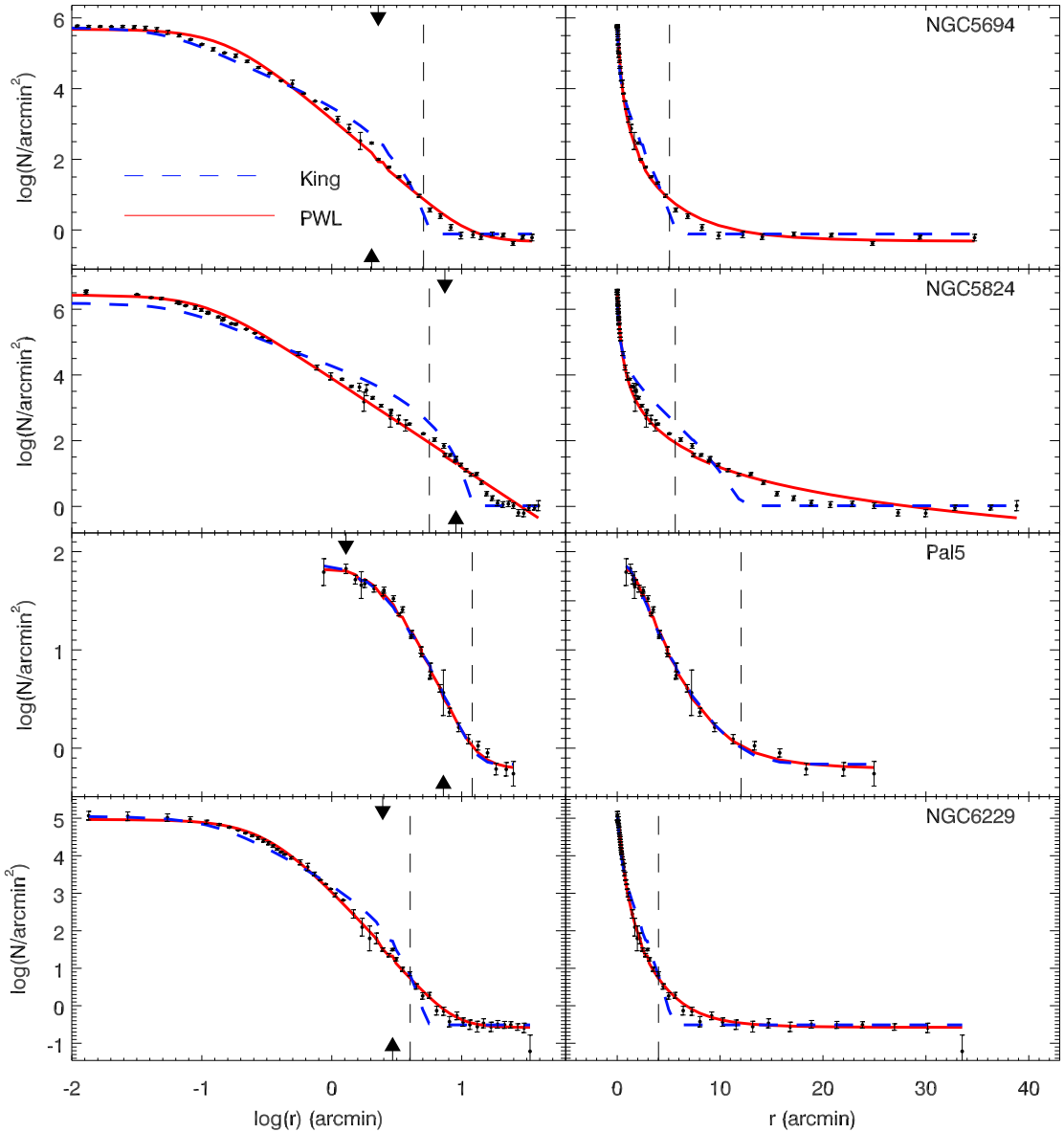


Figure 6. Same as Fig. 3 for NGC 5694, NGC 5824, Pal 5 and NGC 6229.

plate to model a radial profile is that GCs have an infinite extension. Of course we assume that at some point there exists a physical limit at the first Lagrangian point or Jacobi radius.

In the following we analyse the impact that both external and internal factors have in the observed values of γ .

5.2 External factors

It is well known that the structure of a GC is influenced by the interaction with the host Galactic potential (Ostriker et al. 1972; Gnedin & Ostriker 1999; Johnston et al. 1999). In fact, at every passage across the Galactic disc and at every pericentric passage, a transfer of

kinetic energy occurs in the form of compressive (disc) and tidal (bulge) shocks. As a result, the escape of high velocity stars is triggered while the overall energetic budget of the cluster is continuously altered. The theory of the structural evolution of GCs as a result of external tidal effects has been extensively investigated with analytical approximations (Chernoff & Shapiro 1987), through Fokker-Planck modelling (Gnedin & Ostriker 1999) and N -body simulations (Baumgardt & Makino 2003; Gieles & Baumgardt 2008).

It is therefore interesting to check how the strength of these external factors correlates with the shape parameters of our sample of clusters. This task requires the knowledge of the cluster orbits to quantify the impact of the Galactic tidal field. Unfortunately, among the 19 clusters of our sample,

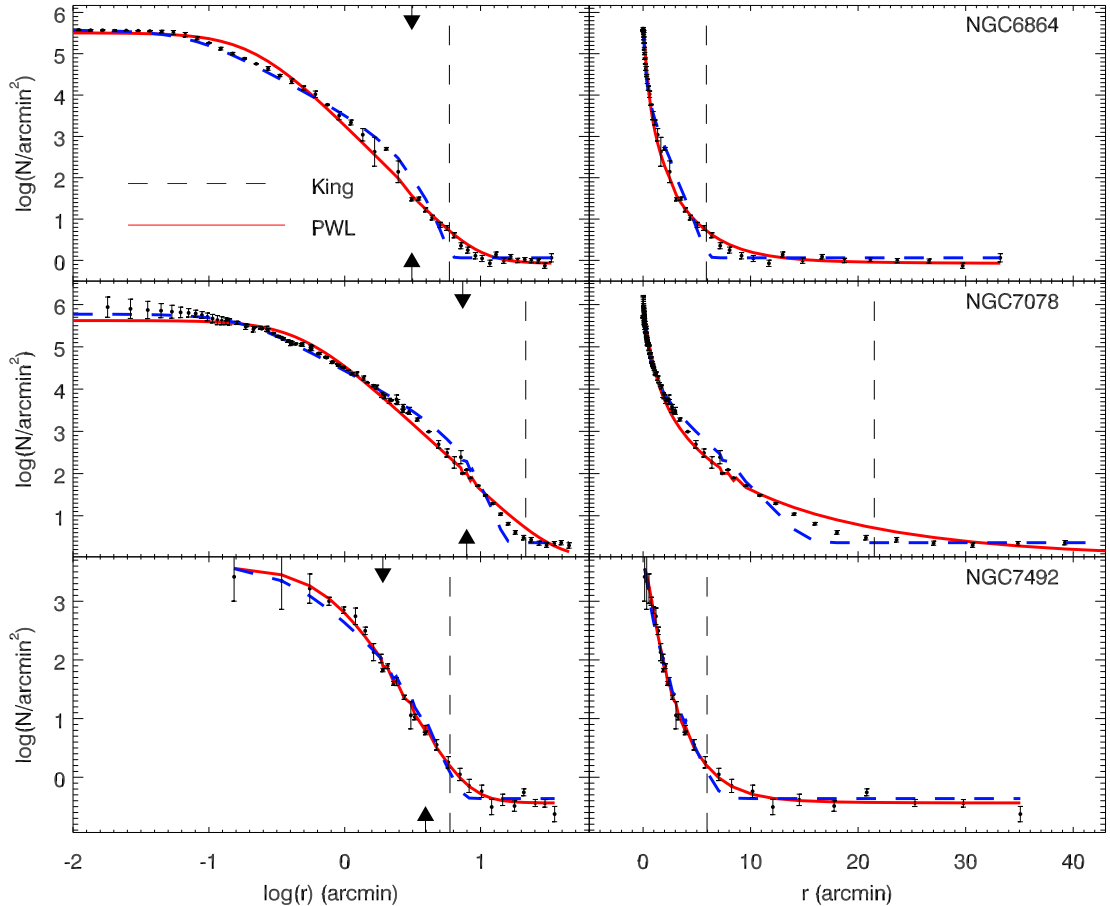


Figure 7. Same as Fig. 3 for NGC 6864, NGC 7078 and NGC 7492 .

only 10 of them have known proper motions so that orbital parameters can be derived only for this subsample.

As a first test we estimated the relative importance of the destruction rate due to relaxation and shocks. For this purpose we adopted the destruction rates due to disc + bulge shocking computed by Allen et al. (2006) and the contribution of relaxation taken from the N -body simulations of Baumgardt & Makino (2003)³. In Figure 10 the ratio $\nu_{\text{disc+bulge}}/\nu_{\text{rlx}}$ is shown for the 10 GCs of our samples with known orbits. For two clusters shocks turn out to be important (Pal 5 and NGC 5466), both belonging to the tidally affected group. For the other GCs (all belonging to the tidally unaffected group) evaporation due to relaxation is the dominant effect. The position of these clusters in the $\gamma - \nu_{\text{disc+bulge}}$ plane is shown in the left panel of Figure 11. It is evident that the two tidally affected clusters, characterized by steeper profiles, are subject to significantly stronger shocks with respect to the group of tidally unaffected clusters.

³ As noticed by Gnedin & Ostriker (1997), the combined effect of shocks and relaxation is generally non-linear. Therefore, although a rigorous decoupling of these two effects is not possible, such an approach must be considered an approximated way to quantify the relative importance of the two effects.

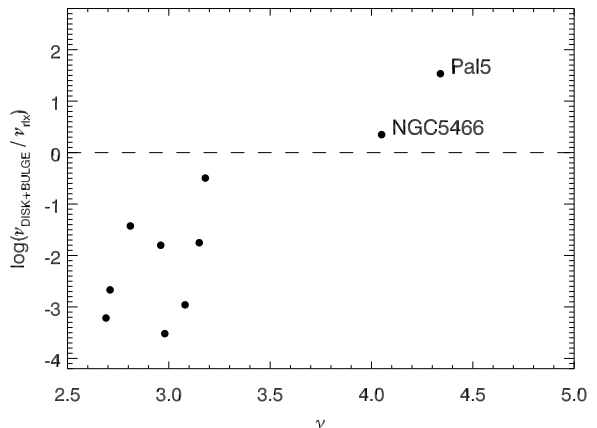


Figure 10. Ratio between the disc+bulge shocking (from Allen et al. 2006) and relaxation from (Baumgardt & Makino 2003) destruction rates as a function of γ . The two clusters belonging to the tidally affected group (Pal 5 and NGC 5466) are indicated.

In absence of accurate orbital parameters it is not possible to check the above correlations for the entire sample of GCs. However, as a general rule, it is expected that the

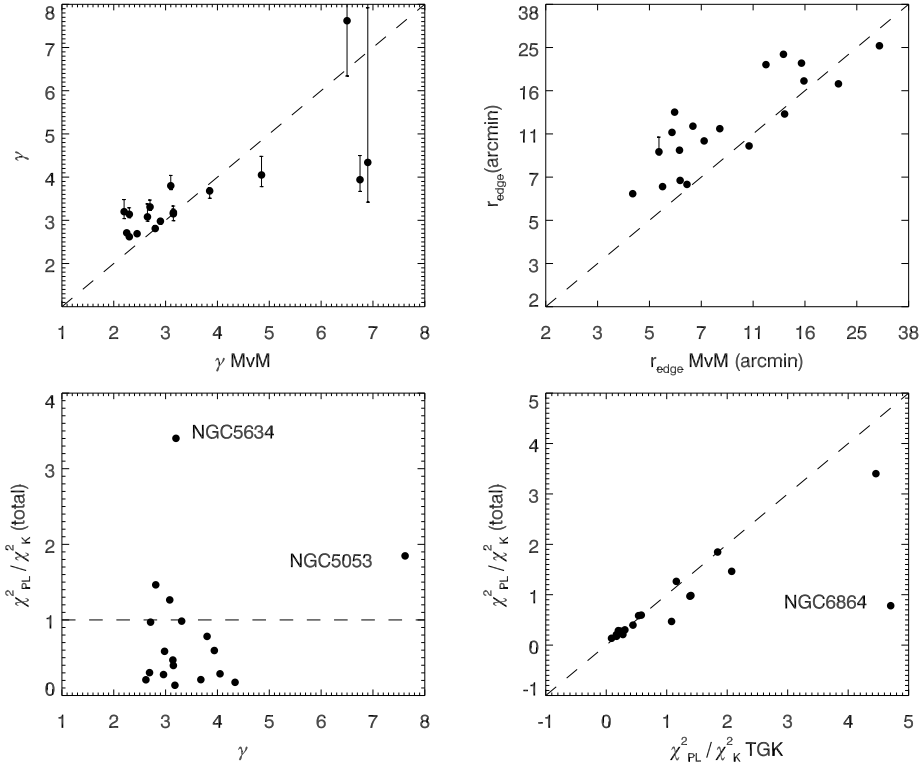


Figure 9. Comparison between our γ (upper-left panel) and r_{edge} (upper-right panel) values with those derived by MvM05. In bottom panels we show the $\chi^2_{\text{PL}} / \chi^2_{\text{K}}$ ratio is shown as a function of γ (bottom-left panel) and the same ratio measured on TGK95 data (bottom-right panel).

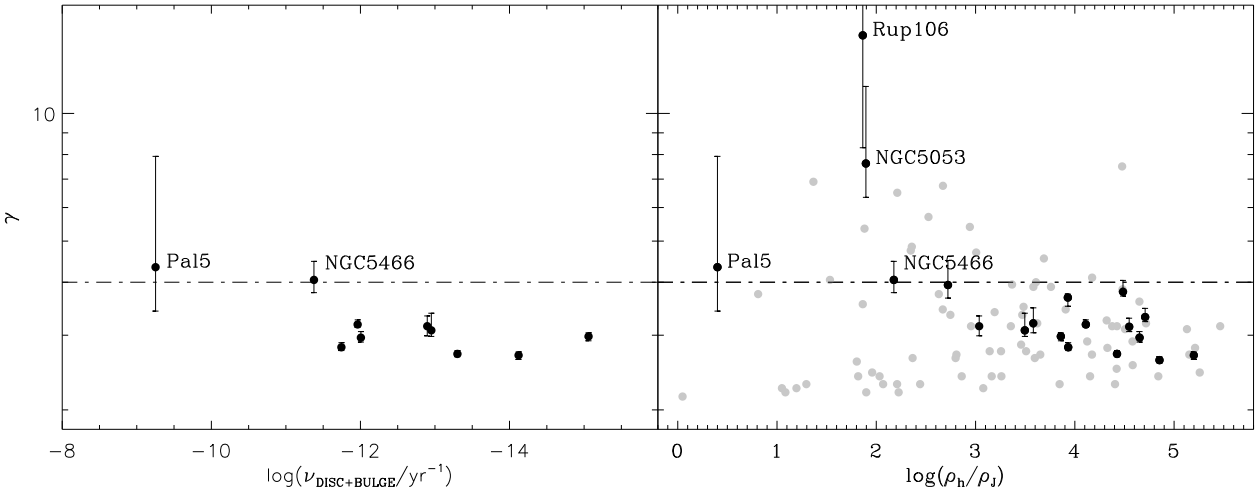


Figure 11. Left: γ parameter as a function of the disc+bulge shocking destruction rate ν from Allen et al. (2006). The two clusters belonging to the tidally affected group (Pal5 and NGC5466) are indicated. Right: variation of γ as a function of ρ_h / ρ_J . The dashed line in both panels indicates the tentative border between the two categories of clusters (at $\gamma = 4$). Grey points mark the sample of Galactic GCs studied by MvM05.

Cluster	$\log(M)$ [M_\odot]	$\log(\rho_h)$ [M_\odot/pc^3]	$\log(t_{\text{rh}})$ [yr]	Power law					King				
				γ	r_0 [']	r_{eff} [']	χ^2_{TGK95}	χ^2_{New}	W_0	r_c [']	r_{eff} [']	χ^2_{TGK95}	χ^2_{New}
NGC 1261	5.20	2.14	9.26	$3.68^{+0.07}_{-0.17}$	0.58	0.67	114.7	67.1	$7.17^{+0.15}_{-0.06}$	0.29	0.92	416.6	449.9
NGC 1851	5.68	3.52	8.99	$2.69^{+0.05}_{-0.06}$	0.16	0.54	131.2	101.6	$8.66^{+0.17}_{-0.09}$	0.11	0.96	221.2	164.4
NGC 1904	5.34	2.64	9.11	$2.71^{+0.05}_{-0.04}$	0.26	0.68	475.5	165.9	$8.06^{+0.07}_{-0.08}$	0.16	0.89	343.8	317.2
NGC 2298	4.59	1.91	8.82	$3.08^{+0.30}_{-0.10}$	0.50	0.65	75.3	32.4	$6.89^{+0.15}_{-0.24}$	0.32	0.90	65.0	20.2
NGC 4147	4.88	2.12	8.97	$2.81^{+0.07}_{-0.05}$	0.19	0.53	781.3	110.7	$7.96^{+0.06}_{-0.12}$	0.10	0.52	376.7	232.7
Rup 106	4.74	0.06	9.89	$15.28^{+4.10}_{-6.98}$	6.56	2.18	-	28.5	$0.51^{+2.43}_{-0.14}$	6.24	2.40	-	79.4
NGC 4590	5.02	1.73	9.33	$3.15^{+0.18}_{-0.16}$	0.95	0.72	49.6	15.3	$7.18^{+0.18}_{-0.13}$	0.56	1.80	112.3	51.5
NGC 5024	5.77	2.06	9.81	$2.98^{+0.06}_{-0.07}$	0.63	0.74	262.8	89.0	$7.56^{+0.09}_{-0.06}$	0.36	1.44	491.6	110.3
NGC 5053	5.07	0.17	9.75	$7.62^{+3.96}_{-1.28}$	4.44	2.35	28.9	13.1	$4.36^{+0.82}_{-0.97}$	1.62	2.09	15.6	7.0
NGC 5272	5.78	2.72	9.48	$3.18^{+0.08}_{-0.05}$	0.77	0.87	95.9	36.3	$8.06^{+0.12}_{-0.10}$	0.36	1.99	441.4	62.6
NGC 5466	4.65	0.51	9.56	$4.05^{+0.43}_{-0.27}$	2.06	2.03	14.1	39.5	$6.58^{+0.37}_{-0.33}$	0.91	2.23	41.9	49.0
NGC 5634	5.26	1.66	9.54	$3.20^{+0.28}_{-0.16}$	0.45	0.62	41.7	59.5	$7.56^{+0.30}_{-0.38}$	0.19	0.77	9.3	20.4
NGC 5694	5.49	2.35	9.41	$3.14^{+0.15}_{-0.08}$	0.16	0.40	70.7	40.3	$8.56^{+0.19}_{-0.19}$	0.06	0.53	44.9	115.8
NGC 5824	5.98	2.76	9.64	$2.62^{+0.05}_{-0.04}$	0.11	0.46	100.3	136.6	$9.45^{+0.21}_{-0.12}$	0.08	1.26	398.0	269.3
Pal 5	4.10	-1.25	9.78	$4.34^{+3.58}_{-0.92}$	3.79	3.41	1.0	9.3	$4.54^{+1.28}_{-1.36}$	2.43	3.25	1.7	15.7
NGC 6229	5.49	2.27	9.46	$3.80^{+0.24}_{-0.09}$	0.32	0.49	19.0	36.0	$7.36^{+0.21}_{-0.15}$	0.14	0.49	112.6	203.0
NGC 6864	5.75	3.11	9.28	$3.31^{+0.66}_{-0.08}$	0.22	0.46	124.5	40.3	$8.16^{+0.20}_{-0.17}$	0.09	0.54	26.4	184.3
NGC 7078	6.14	3.40	9.48	$2.96^{+0.10}_{-0.07}$	0.48	0.77	181.4	54.1	$8.26^{+0.09}_{-0.20}$	0.21	1.39	129.5	109.8
NGC 7492	4.42	0.66	9.30	$3.94^{+0.56}_{-0.27}$	0.81	0.83	10.2	16.9	$6.43^{+0.73}_{-0.62}$	0.39	0.97	43.3	54.9

Table 2. Physical and structural parameters. Masses, densities and half-mass radius relaxation times derived as described in Section 2 and using the new r_h estimations obtained from our best power-law fitting. Ranges of confidence for W_0 and γ have been included to show the discrepancies in some of the clusters, specially Rup 160.

interaction between low-density clusters and the Galaxy become more important because their densities are close to the background density of the Galaxy. In the right panel of Figure 11 we compare the half-mass radius density with the density of field stars within the Jacobi radius calculated as

$$\rho_J \sim 5.376 \left(\frac{R_G}{\text{kpc}} \right)^{-2} M_\odot \text{pc}^{-3} \quad (7)$$

according to appendix B in Gieles et al. (2011). As expected, the tidally affected clusters are restricted to the $\log(\rho_h/\rho_J) < 3$ region of that plot while the rest of $\gamma < 4$ clusters are at least 3 orders of magnitude denser than ρ_J . If we add to our sample those included in MvM05 (grey circles in Figure 11) we find that clusters in the range $\log(\rho_h/\rho_J) \geq 3$ follow the same tendency to be represented by $\gamma < 4$. On the other hand, there is a group of objects at $\log(\rho_h/\rho_J) \sim 1$ and close to $\gamma = 2$ which appear to stray from this behaviour. We will discuss the position of this group of clusters in the next section.

As a further test we also correlated the outer slope parameter γ with the main cluster orbital parameters total energy, z-component of the angular momentum, pericentre radius, orbital period and eccentricity ($E, L_z, R_{\text{peri}}, P$ and e respectively) taken from Dinescu et al. (1999) and constructed an additional parameter $F = (R_G - R_{\text{peri}})/(R_{\text{apo}} - R_{\text{peri}})$ which is an indicator of the current position along the orbit of the clusters. With this definition, $F=1$ when the cluster is at the apocentre while $F=0$ when it is at its pericentre. In these planes the orbits of the two tidally affected clusters are those with the largest eccentricity and the smallest modulus of angular mo-

mentum. This confirms again that eccentric orbits, which make the cluster subject to a significant variation of the surrounding external field, can lead clusters toward the evaporation regime. A group of tidally unaffected clusters exhibit orbits with similar eccentricities and angular momentum. It is interesting to note that all these clusters have been suspected to be accreted (e.g. NGC1851, NGC1904, NGC2298 and NGC4147; Forbes & Bridges 2010) or are very massive (NGC7078). Accreted clusters might have different evolutionary histories from Galactic GCs, passing a significant part of their evolution in smaller systems as dwarf galaxies before the accretion, so this could explain why accreted and in-situ clusters present a different overall structure, even if they have similar orbital parameters. Mass represents also an important parameter since massive clusters could resist the strong tidal interaction that lead towards high gamma values. As we have commented, clusters on highly-eccentric orbits as NGC 5466 and Pal 5 are influenced by the interaction with the Milky Way significantly, leading to the formation of an external (and different) power-law distribution. No other significant trends are visible in the plots shown in Figure 12 between γ and the other orbital parameters.

5.3 Internal evolution

After evaluating the influence of external factors on the observed number density profiles, we looked at the correlations between the general physical parameters of the cluster with the slope γ . As in stellar physics, the global mass is always one of the first suspects to drive the behaviour of the struc-

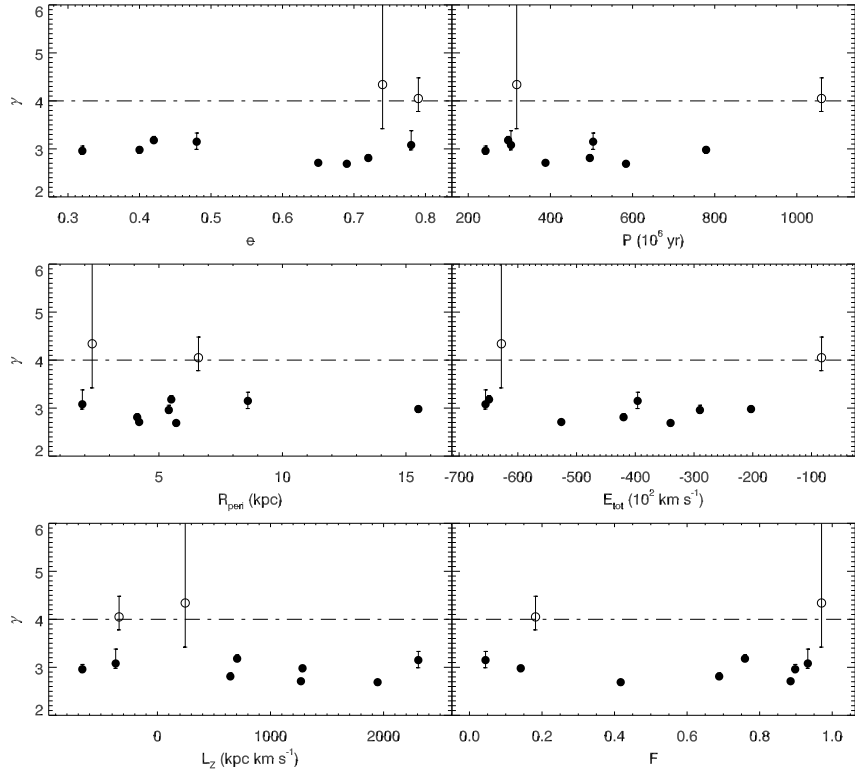


Figure 12. γ as a function of the orbital parameters: eccentricity (upper left panel), period (upper right panel), pericentric distance (middle left panel), energy (middle right panel), angular momentum (bottom left panel) and phase (bottom right panel). The location of the two clusters of the tidally affected group (Pal 5 and NGC 5466) are indicated in each panel with open circles.

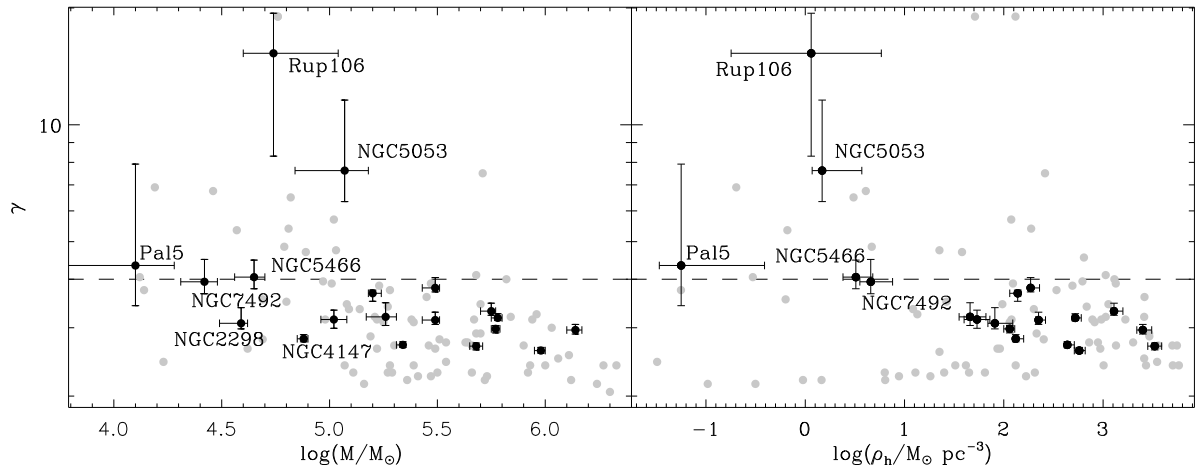


Figure 13. γ as a function of mass and density. The dashed line in both panels indicates the tentative border between the two categories of clusters (at $\gamma = 4$). Grey points mark the sample of Galactic GCs studied by MvM05.

ture of a GC and we have tested this correlation in the left panel of Figure 13.

It has been already noticed (Section 4) that all the clusters of the tidally unaffected subsample, formed by massive clusters, present flatter radial profiles while the less massive tidally affected clusters have large values of γ . A similar relation was found by McLaughlin (2000) using in that case the concentration $\log(r_{\text{edge}}/r_c)$ as a function of the cluster luminosity.

A possible interpretation of this behaviour can be searched by looking at the role of binaries in the long-term evolution of GCs. Low-mass clusters are able to form and retain more binaries than massive clusters where they are more efficiently destroyed in single-binary and binary-binary close encounters (Giersz & Spurzem 1994; Sollima 2008; Fregeau et al. 2009). While the natural evolution of GCs is toward high-concentration structures (Hénon 1961) a large fraction of binaries prevent the contraction of the core and maintain the cluster in a quasi-steady state of binary burning where the continuous loss of energy due to evaporation is balanced by the energy heating of binaries (Gao et al. 1991; Vesperini 1998; Fregeau & Rasio 2007). Unfortunately, the binary fraction has only been estimated for NGC 4590 (tidally unaffected), NGC 5053 and NGC 5466 (tidally affected) (see Sollima et al. 2007) and appear to cover the same range ($9.5 < \xi < 14.2\%$) within the errors. Although the available data do not allow to confirm the scenario proposed above, other studies have suggested an anti-correlation between the mass and the fraction of binary systems in larger samples of Galactic GCs (Milone et al. 2008; Sollima 2008; Sollima et al. 2010). In addition, mass loss due to stellar evolution drives the dynamical evolution in early stages and causes low-mass stellar systems to expand to their tidal boundary faster than their more massive counter-parts (Gieles et al. 2010). This, together with the external factors discussed in the previous section, could explain the tendency found in the low-mass tidally affected clusters to have prominent cores, large half-mass radii and larger values of γ .

We have to analyse the exception of NGC 2298 and NGC 4147 in the γ vs. $\log(M)$ plot. Despite their low masses, these clusters are included in the tidally unaffected group according to Table 2. Special birth conditions or an external origin could explain these differences. This last hypothesis has been widely supported for NGC 4147 (Bellazzini et al. 2003; Forbes & Bridges 2010) since it lies in the projected position path of the Sagittarius tidal stream sharing the same energy and angular momentum. Similarly, NGC 2298 has been associated to the controversial Canis Major dwarf galaxy (Martin et al. 2004; Forbes & Bridges 2010) although it presents a retrograde orbit incompatible with that of this over-density but also with the general rotational pattern of the Milky Way. In this picture, GCs formed in less dense systems, might live as isolated (tidally unaffected) clusters before the accretion by the Milky Way.

The derived outer slope γ vs. the half-mass density ρ_h is shown on the right panel of Figure 13. Also in this case, a striking correlation is evident in the sense that denser clusters have on average flatter profiles. In this case, denser clusters are both expected to be more resistant to the external tidal stress exerted by the Milky Way (see Section 5.2) and dominated by the effect of relaxation (eq. 2). In Figure 13 we have also included the sample of clusters studied by MvM05.

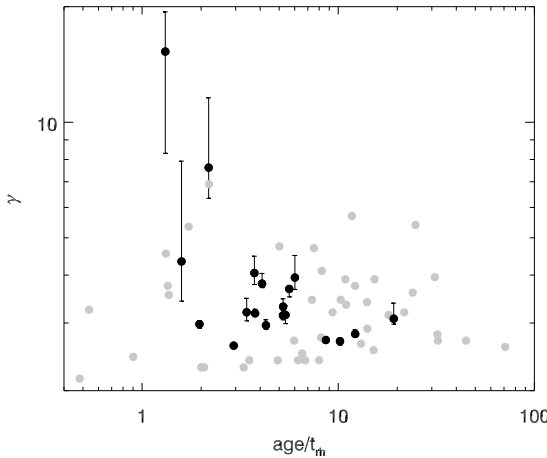


Figure 14. γ as a function of age/t_{rh} . Grey dots mark the Galactic GCs of the MvdM sample.

The trend found in the relations between mass, half mass density and γ are also visible here although the presence of a branch of massive clusters with $\gamma \sim 2$ and reaching very low densities decreases the significance of the $\gamma - \rho_h$ correlation.

Of course, the MvM05 sample contains an order of magnitude larger number of objects and constitutes a more robust statistical sample to check such correlations. However, it is noticeable that for most of these object the TGK95 profiles cover a very limited FOV (including only the first central arcminutes). As shown in Section 4, an incomplete radial coverage can significantly alter the estimate of the profile slope leading to a more uncertain determination of both γ and ρ_h . It is therefore possible that the surprisingly low half-mass density of these object is due to an underestimate of γ and, consequently, ρ_h .

Connecting the structure of our sample of Galactic GCs with their dynamical age is not simple because of their narrow range of relative ages (Marín-Franch et al. 2009). In Figure 14, we show the parameter γ as a function of the ratio age/t_{rh} . On average, clusters with lower ratios of age/t_{rh} have larger values of γ even if the large scatter prevents from any firm conclusion on the existence of any reliable correlation. The same behaviour is visible among the clusters in the MvM05 sample with the exception of the group of globulars with $\gamma \sim 2$ already mentioned above which show a lower age/t_{rh} . It is difficult to say something about the relation between γ and the dynamical age of clusters. This is firstly because clusters in the tidally unaffected regime have expanded such that their relaxation times have become a fixed fraction of their age, roughly equal to $\sim 1/10$ for clusters of equal masses (Hénon 1965; Goodman 1984) and $\sim 1/3$ for clusters with a globular type stellar mass-function (Gieles et al. 2011). The majority of clusters in our sample is in this regime and forms a cloud of points in Fig. 14. Secondly, the evolution of clusters with an age roughly equal to t_{rh} is probably driven by external factors due to their low density, hence t_{rh} is not telling us much about the evolution for these objects.

6 CONCLUSIONS

We have presented the number density profiles of 19 Galactic GCs obtained with deep wide-field photometry. The comparison of our results, fitting both King models and power-law templates, with those derived by previous studies shows the importance that data with a wider FOVs have on our understanding of these stellar systems. In particular, the edge radii estimated from this analysis have been found to be $\sim 20\%$ larger than what found in previous works based on shallower surface brightness profile. The number density profiles of our sample of GCs can be reasonably fitted by both King models and power-law templates. The latter ones appear to be a better representation for $\sim 2/3$ of the observed profiles including some of those clusters showing evidences of tidal tails (Pal 5 and NGC 5466, Odenkirchen et al. 2001; Belokurov et al. 2006), in agreement with the prediction of N -body simulations (Lee et al. 2006; Peñarrubia et al. 2009; Johnston et al. 1999).

It has been found that the slope γ is linked to the membership of the cluster to the group of "tidally affected" or "tidally unaffected" clusters (defined by Gieles et al. (2011) on the basis of the position in the $\rho_h(M, R_G)$ plane). The group of tidally affected clusters, constituted mainly of low-mass objects with prominent cores, is characterized by steeper profiles ($\gamma > 4$) while tidally unaffected clusters show flatter profiles extending to large distances from their compact cores.

We investigated the dependence of the outer slope of the density profile γ on the internal structural evolution of the cluster (based on the relaxation process) and on external factors (i.e. tidal shocks) using a subsample of 10 GCs with known orbits. External factors have been found to be dominant in the two tidally affected clusters (Pal 5 and NGC 5466), which have preferentially more eccentric orbits and larger destruction rates than tidally unaffected clusters. This finding agree with the evidence of massive tidal tails around these two clusters (see above) indicating their strong interaction with the Galactic potential. For the other clusters of the sample, internal processes can be considered the main mechanisms of dynamical evolution.

We revealed a slight correlation between γ and the cluster mass and half-mass density which can be interpreted as a consequence of the fact that the most massive and dense tidally unaffected clusters are currently in an expansion dominated phase (Gieles et al. 2011). The connection between slope γ and half-mass density is less significant in the larger sample by MvM05 which is however limited to the innermost fit of the clusters. It is therefore not clear if such a relation is spurious (due to the small number of clusters of our sample) or real (and masked by the presence of outliers in the MvM05 sample).

ACKNOWLEDGEMENTS

Based on observations made with the Isaac Newton Telescope operated on the island of La Palma by the Isaac Newton Group in the Spanish Observatorio del Roque de los Muchachos of the Instituto de Astrofísica de Canarias and with 2.2 m ESO telescope at the La Silla Observatory under programme IDs 082.B-0386, 084.B-0666 and 085.B-0765. We warmly thank the anonymous referee for his/her

helpful comments and suggestions. We also thank Liliya L. R. Williams for her comments. MG acknowledges financial support from the Royal Society. JP acknowledges support from the STFC-funded Galaxy Formation and Evolution programme at the IoA.

REFERENCES

Allen C., Moreno E., Pichardo B., 2006, *ApJ*, 652, 1150
 Baraffe I., Chabrier G., Allard F., Hauschildt P. H., 1998, *A&A*, 337, 403
 Bastian N., Gieles M., Goodwin S. P., Tranchant G., Smith L. J., Konstantopoulos I., Efremov Y., 2008, *MNRAS*, 389, 223
 Baumgardt H., 2001, *MNRAS*, 325, 1323
 Baumgardt H., Makino J., 2003, *MNRAS*, 340, 227
 Baumgardt H., Parmentier G., Gieles M., Vesperini E., 2010, *MNRAS*, 401, 1832
 Bellazzini M., Ferraro F. R., Ibata R., 2003, *AJ*, 125, 188
 Bellazzini M., Fusi Pecci F., Messineo M., Monaco L., Rood R. T., 2002, *AJ*, 123, 1509
 Bellazzini M., Ibata R., Ferraro F. R., 2004, in F. Prada, D. Martinez Delgado, & T. J. Mahoney ed., Satellites and Tidal Streams Vol. 327 of Astronomical Society of the Pacific Conference Series, Globular Clusters in the Sgr Stream and Other Structures. pp 220–+
 Belokurov V., Evans N. W., Irwin M. J., Hewett P. C., Wilkinson M. I., 2006, *ApJL*, 637, L29
 Binney J., Merrifield M., 1998, Galactic Astronomy
 Borissova J., Catelan M., Ferraro F. R., Spassova N., Buonanno R., Iannicola G., Richtler T., Sweigart A. V., 1999, *A&A*, 343, 813
 Brodie J. P., Strader J., 2006, *ARA&A*, 44, 193
 Carraro G., 2009, *AJ*, 137, 3809
 Carraro G., Zinn R., Moni Bidin C., 2007, *A&A*, 466, 181
 Chernoff D. F., Shapiro S. L., 1987, *ApJ*, 322, 113
 Correnti M., Bellazzini M., Dalessandro E., Mucciarelli A., Monaco L., Catelan M., 2011, arXiv:1105.2001
 Côté P., Djorgovski S. G., Meylan G., Castro S., McCarthy J. K., 2002, *ApJ*, 574, 783
 Dehnen W., Odenkirchen M., Grebel E. K., Rix H.-W., 2004, *AJ*, 127, 2753
 Dinescu D. I., Girard T. M., van Altena W. F., 1999, *AJ*, 117, 1792
 Djorgovski S., King I. R., 1986, *ApJL*, 305, L61
 Elson R. A. W., Fall S. M., Freeman K. C., 1987, *ApJ*, 323, 54
 Elson R. A. W., Freeman K. C., Lauer T. R., 1989, *ApJL*, 347, L69
 Forbes D. A., Bridges T., 2010, *MNRAS*, 404, 1203
 Fregeau J. M., Ivanova N., Rasio F. A., 2009, *ApJ*, 707, 1533
 Fregeau J. M., Rasio F. A., 2007, *ApJ*, 658, 1047
 Fukushige T., Heggie D. C., 2000, *MNRAS*, 318, 753
 Gao B., Goodman J., Cohn H., Murphy B., 1991, *ApJ*, 370, 567
 Gieles M., Baumgardt H., 2008, *MNRAS*, 389, L28
 Gieles M., Baumgardt H., Heggie D. C., Lamers H. J. G. L. M., 2010, *MNRAS*, 408, L16
 Gieles M., Heggie D. C., Zhao H., 2011, *MNRAS*, 413, 2509
 Giersz M., Heggie D. C., 1994, *MNRAS*, 268, 257

Giersz M., Spurzem R., 1994, *MNRAS*, 269, 241

Gnedin O. Y., Ostriker J. P., 1997, *ApJ*, 474, 223

Gnedin O. Y., Ostriker J. P., 1999, *ApJ*, 513, 626

Goodman J., 1984, *ApJ*, 280, 298

Harris W. E., 1996, *AJ*, 112, 1487

Harris W. E., 2010, arXiv:1012.3224

Hénon M., 1961, *Annales d'Astrophysique*, 24, 369

Hénon M., 1965, *Annales d'Astrophysique*, 28, 62

Hut P., McMillan S., Goodman J., Mateo M., Phinney E. S., Pryor C., Richer H. B., Verbunt F., Weinberg M., 1992, *PASP*, 104, 981

Innanen K. A., Harris W. E., Webbink R. F., 1983, *AJ*, 88, 338

Johnston K. V., Sigurdsson S., Hernquist L., 1999, *MNRAS*, 302, 771

Jordi K., Grebel E. K., 2010, *A&A*, 522, A71+

King I., 1962, *AJ*, 67, 471

King I. R., 1966, *AJ*, 71, 64

Küpper A. H. W., Kroupa P., Baumgardt H., Heggie D. C., 2010, *MNRAS*, 407, 2241

Landolt A. U., 1992, *AJ*, 104, 340

Larsen S. S., 2004, *A&A*, 416, 537

Lauchner A., Powell Jr. W. L., Wilhelm R., 2006, *ApJL*, 651, L33

Lee H. M., Ostriker J. P., 1987, *ApJ*, 322, 123

Lee K. H., Lee H. M., Sung H., 2006, *MNRAS*, 367, 646

Leon S., Meylan G., Combes F., 2000, *A&A*, 359, 907

Mackey A. D., Gilmore G. F., 2003a, *MNRAS*, 338, 120

Mackey A. D., Gilmore G. F., 2003b, *MNRAS*, 338, 85

Mackey A. D., Wilkinson M. I., Davies M. B., Gilmore G. F., 2008, *MNRAS*, 386, 65

Mackey et al. 2010, *MNRAS*, 401, 533

Maíz-Apellániz J., 2001, *ApJ*, 563, 151

Marigo P., Girardi L., Bressan A., Groenewegen M. A. T., Silva L., Granato G. L., 2008, *A&A*, 482, 883

Marín-Franch A., Aparicio A., Piotto G., Rosenberg A., Chaboyer B., Sarajedini A., Siegel M., Anderson J., Bedin L. R., Dotter A., Hempel M., King I., Majewski S., Milone A. P., Paust N., Reid I. N., 2009, *ApJ*, 694, 1498

Martin N. F., Ibata R. A., Bellazzini M., Irwin M. J., Lewis G. F., Dehnen W., 2004, *MNRAS*, 348, 12

Martínez-Delgado D., Dinescu D. I., Zinn R., Tutsoff A., Côté P., Boyarchuck A., 2004, in F. Prada, D. Martínez Delgado, & T. J. Mahoney ed., *Satellites and Tidal Streams* Vol. 327 of *Astronomical Society of the Pacific Conference Series*, *Mapping Tidal Streams around Galactic Globular Clusters*. pp 255–+

McLaughlin D. E., 2000, *ApJ*, 539, 618

McLaughlin D. E., van der Marel R. P., 2005, *ApJS*, 161, 304

Meylan G., Heggie D. C., 1997, *A&A Rev.*, 8, 1

Michie R. W., 1963, *MNRAS*, 126, 499

Milone A. P., Piotto G., Bedin L. R., Sarajedini A., 2008, *Mem. Soc. Astron. Italiana*, 79, 623

Niederste-Ostholt M., Belokurov V., Evans N. W., Koposov S., Gieles M., Irwin M. J., 2010, *MNRAS*, 408, L66

Noyola E., Gebhardt K., 2006, *AJ*, 132, 447

Odenkirchen M., Grebel E. K., Dehnen W., Rix H., Yanny B., Newberg H. J., Rockosi C. M., Martínez-Delgado D., Brinkmann J., Pier J. R., 2003, *ApJ*, 126, 2385

Odenkirchen et al. 2001, *ApJL*, 548, L165

Oh K. S., Lin D. N. C., Aarseth S. J., 1995, *ApJ*, 442, 142

Olszewski E. W., Saha A., Knezeck P., Subramaniam A., de Boer T., Seitzer P., 2009, *AJ*, 138, 1570

Ostriker J. P., Spitzer L. J., Chevalier R. A., 1972, *ApJL*, 176, L51+

Peñarrubia J., Navarro J. F., McConnachie A. W., Martin N. F., 2009, *ApJ*, 698, 222

Plummer H. C., 1911, *MNRAS*, 71, 460

Searle L., Zinn R., 1978, *ApJ*, 225, 357

Sollima A., 2008, *MNRAS*, 388, 307

Sollima A., Beccari G., Ferraro F. R., Fusi Pecci F., Sarajedini A., 2007, *MNRAS*, 380, 781

Sollima A., Carballo-Bello J. A., Beccari G., Ferraro F. R., Faccioli P. F., Lanzoni B., 2010, *MNRAS*, 401, 577

Sollima A., Martínez-Delgado D., Valls-Gabaud D., Peñarrubia J., 2011, *ApJ*, 726, 47

Spitzer L., 1987, *Dynamical evolution of globular clusters*. Princeton, NJ, Princeton University Press, 1987, 191 p.

Spitzer L. J., Hart M. H., 1971, *ApJ*, 164, 399

Stetson P. B., 1987, *PASP*, 99, 191

Testa V., Zaggia S. R., Andreon S., Longo G., Scaramella R., Djorgovski S. G., de Carvalho R., 2000, *A&A*, 356, 127

Trager S. C., King I. R., Djorgovski S., 1995, *AJ*, 109, 218

Vesperini E., 1998, *MNRAS*, 299, 1019

Vesperini E., Heggie D. C., 1997, *MNRAS*, 289, 898

Walker et al. 2011, *MNRAS*, 415, 643

Wilkinson M. I., Hurley J. R., Mackey A. D., Gilmore G. F., Tout C. A., 2003, *MNRAS*, 343, 1025

Wilson C. P., 1975, *AJ*, 80, 175

Woolley R. V. D. R., Robertson D. A., 1956, *MNRAS*, 116, 288

Zepf S. E., Ashman K. M., 1993, *MNRAS*, 264, 611

Zhao H., 1996, *MNRAS*, 278, 488

Zinn R., 1993, in G. H. Smith & J. P. Brodie ed., *The Globular Cluster-Galaxy Connection* Vol. 48 of *Astronomical Society of the Pacific Conference Series*, *The Galactic Halo Cluster Systems: Evidence for Accretion*. pp 38–+